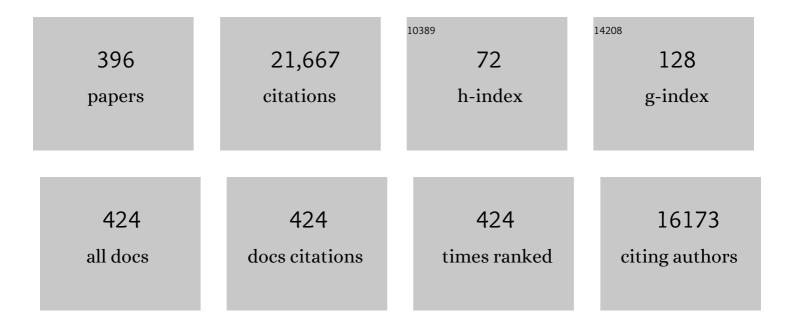
Richard E Carson

List of Publications by Year in descending order

Source: https://exaly.com/author-pdf/6863997/publications.pdf Version: 2024-02-01



| # | Article | IF | CITATIONS |
|----|--|-----|-----------|
| 1 | Feasibility study of PET dynamic imaging of [18F]DHMT for quantification of reactive oxygen species in the myocardium of large animals. Journal of Nuclear Cardiology, 2022, 29, 216-225. | 2.1 | 5 |
| 2 | Optimized Methodology for Reference Region and Image-Derived Input Function Kinetic Modeling in Preclinical PET. IEEE Transactions on Radiation and Plasma Medical Sciences, 2022, 6, 454-462. | 3.7 | 2 |
| 3 | Imaging Pituitary Vasopressin 1B Receptor in Humans with the PET Radiotracer ¹¹ C-TASP699. Journal of Nuclear Medicine, 2022, 63, 609-614. | 5.0 | 7 |
| 4 | Glia Imaging Differentiates Multiple System Atrophy from Parkinson's Disease: A Positron Emission Tomography Study with [<scp>¹¹C</scp>] <scp>PBR28</scp> and Machine Learning Analysis. Movement Disorders, 2022, 37, 119-129. | 3.9 | 18 |
| 5 | Association of entorhinal cortical tau deposition and hippocampal synaptic density in older individuals with normal cognition and early Alzheimer's disease. Neurobiology of Aging, 2022, 111, 44-53. | 3.1 | 25 |
| 6 | A metabolically stable PET tracer for imaging synaptic vesicle protein 2A: synthesis and preclinical characterization of [18F]SDM-16. European Journal of Nuclear Medicine and Molecular Imaging, 2022, 49, 1482-1496. | 6.4 | 16 |
| 7 | Lower prefrontal cortical synaptic vesicle binding in cocaine use disorder: An exploratory ¹¹ Câ€UCBâ€J positron emission tomography study in humans. Addiction Biology, 2022, 27, e13123. | 2.6 | 16 |
| 8 | Translational PET Imaging of Spinal Cord Injury with the Serotonin Transporter Tracer [11C]AFM. Molecular Imaging and Biology, 2022, , 1. | 2.6 | 0 |
| 9 | Characterization in nonhuman primates of (R)-[18F]OF-Me-NB1 and (S)-[18F]OF-Me-NB1 for imaging the GluN2B subunits of the NMDA receptor. European Journal of Nuclear Medicine and Molecular Imaging, 2022, , 1. | 6.4 | 8 |
| 10 | Comparison of three novel radiotracers for GluN2B-containing NMDA receptors in non-human primates: <i>(R)</i> -[¹¹ C]NR2B-Me, <i>(R)</i> -[¹⁸ F]of-Me-NB1, and <i>(S)</i> -[¹⁸ F]of-NB1. Journal of Cerebral Blood Flow and Metabolism, 2022, 42, 1398-1409. | 4.3 | 7 |
| 11 | Synaptic density and cognitive performance in Alzheimer's disease: A PET imaging study with [¹¹ C]UCBâ€J. Alzheimer's and Dementia, 2022, 18, 2527-2536. | 0.8 | 55 |
| 12 | Imaging the effect of ketamine on synaptic density (SV2A) in the living brain. Molecular Psychiatry, 2022, 27, 2273-2281. | 7.9 | 25 |
| 13 | Target occupancy study and whole-body dosimetry with a MAGL PET ligand [11C]PF-06809247 in non-human primates. EJNMMI Research, 2022, 12, 13. | 2.5 | 1 |
| 14 | PET-BIDS, an extension to the brain imaging data structure for positron emission tomography. Scientific Data, 2022, 9, 65. | 5.3 | 20 |
| 15 | Multimodal neuroimaging of metabotropic glutamate 5 receptors and functional connectivity in alcohol use disorder. Alcoholism: Clinical and Experimental Research, 2022, , . | 2.4 | Ο |
| 16 | PET Imaging of Synaptic Density: Challenges and Opportunities of Synaptic Vesicle Glycoprotein 2A PET in Small Animal Imaging. Frontiers in Neuroscience, 2022, 16, 787404. | 2.8 | 5 |
| 17 | Adaptive data-driven motion detection and optimized correction for brain PET. NeuroImage, 2022, 252, 119031. | 4.2 | 8 |
| 18 | Feasibility of imaging synaptic density in the human spinal cord using [11C]UCB-J PET. EJNMMI Physics, 2022, 9, 32. | 2.7 | 3 |

| # | Article | IF | CITATIONS |
|----|--|------|-----------|
| 19 | Imaging the fetal nonhuman primate brain with SV2A positron emission tomography (PET). European Journal of Nuclear Medicine and Molecular Imaging, 2022, 49, 3679-3691. | 6.4 | 4 |
| 20 | Reversal of synapse loss in Alzheimer mouse models by targeting mGluR5 to prevent synaptic tagging by C1Q. Science Translational Medicine, 2022, 14, . | 12.4 | 38 |
| 21 | Imaging of Synaptic Density in Neurodegenerative Disorders. Journal of Nuclear Medicine, 2022, 63, 605-675. | 5.0 | 29 |
| 22 | Accelerating PET Image Reconstruction with CUDA. , 2022, , . | | 0 |
| 23 | Preliminary in vivo evidence of lower hippocampal synaptic density in cannabis use disorder. Molecular Psychiatry, 2021, 26, 3192-3200. | 7.9 | 32 |
| 24 | Binding of the synaptic vesicle radiotracer [¹¹ C]UCB-J is unchanged during functional brain activation using a visual stimulation task. Journal of Cerebral Blood Flow and Metabolism, 2021, 41, 1067-1079. | 4.3 | 28 |
| 25 | Simplified Quantification of ¹¹ C-UCB-J PET Evaluated in a Large Human Cohort. Journal of Nuclear Medicine, 2021, 62, 418-421. | 5.0 | 19 |
| 26 | First-in-Human Evaluation of ¹⁸ F-SynVesT-1, a Radioligand for PET Imaging of Synaptic Vesicle Glycoprotein 2A. Journal of Nuclear Medicine, 2021, 62, 561-567. | 5.0 | 60 |
| 27 | Multimodal investigation of dopamine D2/D3 receptors, default mode network suppression, and cognitive control in cocaine-use disorder. Neuropsychopharmacology, 2021, 46, 316-324. | 5.4 | 14 |
| 28 | Acute neuroimmune stimulation impairs verbal memory in adults: A PET brain imaging study. Brain, Behavior, and Immunity, 2021, 91, 784-787. | 4.1 | 6 |
| 29 | Quantification of SV2A Binding in Rodent Brain Using [18F]SynVesT-1 and PET Imaging. Molecular Imaging and Biology, 2021, 23, 372-381. | 2.6 | 20 |
| 30 | Longitudinal imaging of metabotropic glutamate 5 receptors during early and extended alcohol abstinence. Neuropsychopharmacology, 2021, 46, 380-385. | 5.4 | 7 |
| 31 | First-in-Human Assessment of ¹¹ C-LSN3172176, an M1 Muscarinic Acetylcholine Receptor PET Radiotracer. Journal of Nuclear Medicine, 2021, 62, 553-560. | 5.0 | 35 |
| 32 | PET Imaging Estimates of Regional Acetylcholine Concentration Variation in Living Human Brain. Cerebral Cortex, 2021, 31, 2787-2798. | 2.9 | 5 |
| 33 | Association of Aβ deposition and regional synaptic density in early Alzheimer's disease: a PET imaging study with [11C]UCB-J. Alzheimer's Research and Therapy, 2021, 13, 11. | 6.2 | 53 |
| 34 | Assessment of test-retest reproducibility of [18F]SynVesT-1, a novel radiotracer for PET imaging of synaptic vesicle glycoprotein 2A. European Journal of Nuclear Medicine and Molecular Imaging, 2021, 48, 1327-1338. | 6.4 | 23 |
| 35 | Dopamine D2/3 receptor availability in cocaine use disorder individuals with obesity as measured by [11C]PHNO PET. Drug and Alcohol Dependence, 2021, 220, 108514. | 3.2 | 1 |
| 36 | Comparison of [¹¹ C]UCB-J and [¹⁸ F]FDG PET in Alzheimer's disease: A tracer kinetic modeling study. Journal of Cerebral Blood Flow and Metabolism, 2021, 41, 2395-2409. | 4.3 | 43 |

| # | Article | IF | CITATIONS |
|----|---|-----|-----------|
| 37 | Preliminary In Vivo Evidence of Reduced Synaptic Density in Human Immunodeficiency Virus (HIV) Despite Antiretroviral Therapy. Clinical Infectious Diseases, 2021, 73, 1404-1411. | 5.8 | 25 |
| 38 | In vivo evidence of lower synaptic vesicle density in schizophrenia. Molecular Psychiatry, 2021, 26, 7690-7698. | 7.9 | 51 |
| 39 | Generation of synthetic PET images of synaptic density and amyloid from ¹⁸ Fâ€FDG images using deep learning. Medical Physics, 2021, 48, 5115-5129. | 3.0 | 12 |
| 40 | Multiparametric cardiac 18F-FDG PET in humans: pilot comparison of FDG delivery rate with 82Rb myocardial blood flow. Physics in Medicine and Biology, 2021, 66, 155015. | 3.0 | 3 |
| 41 | Lower synaptic density is associated with psychiatric and cognitive alterations in obesity. Neuropsychopharmacology, 2021, , . | 5.4 | 7 |
| 42 | Generation of parametric <i>K</i> _i images for FDG PET using two 5â€min scans. Medical Physics, 2021, 48, 5219-5231. | 3.0 | 16 |
| 43 | Identifying brain networks in synaptic density PET (11C-UCB-J) with independent component analysis. NeuroImage, 2021, 237, 118167. | 4.2 | 18 |
| 44 | Effect of age on brain metabotropic glutamate receptor subtype 5 measured with [18F]FPEB PET. NeuroImage, 2021, 238, 118217. | 4.2 | 10 |
| 45 | Partial volume correction analysis for 11C-UCB-J PET studies of Alzheimer's disease. NeuroImage, 2021, 238, 118248. | 4.2 | 17 |
| 46 | Novel Reversible-Binding PET Ligands for Imaging Monoacylglycerol Lipase Based on the Piperazinyl Azetidine Scaffold. Journal of Medicinal Chemistry, 2021, 64, 14283-14298. | 6.4 | 9 |
| 47 | Synthesizing Multi-tracer PET Images for Alzheimer's Disease Patients Using a 3D Unified Anatomy-Aware Cyclic Adversarial Network. Lecture Notes in Computer Science, 2021, , 34-43. | 1.3 | 6 |
| 48 | PET Imaging of Synaptic Vesicle Protein 2A. , 2021, , 993-1019. | | 10 |
| 49 | Imaging brain cortisol regulation in PTSD with a target for 11β-hydroxysteroid dehydrogenase type 1. Journal of Clinical Investigation, 2021, 131, . | 8.2 | 10 |
| 50 | Data-driven analysis of kappa opioid receptor binding in major depressive disorder measured by positron emission tomography. Translational Psychiatry, 2021, 11, 602. | 4.8 | 1 |
| 51 | Quantification of PET infusion studies without true equilibrium: A tissue clearance correction. Journal of Cerebral Blood Flow and Metabolism, 2020, 40, 860-874. | 4.3 | 6 |
| 52 | Parametric Imaging With PET and SPECT. IEEE Transactions on Radiation and Plasma Medical Sciences, 2020, 4, 1-23. | 3.7 | 43 |
| 53 | First in-human PET study and kinetic evaluation of [¹⁸ F]AS2471907 for imaging 11β-hydroxysteroid dehydrogenase type 1. Journal of Cerebral Blood Flow and Metabolism, 2020, 40, 695-704. | 4.3 | 10 |
| 54 | Direct List Mode Parametric Reconstruction for Dynamic Cardiac SPECT. IEEE Transactions on Medical Imaging, 2020, 39, 119-128. | 8.9 | 7 |

| # | Article | IF | CITATIONS |
|----|---|-----|-----------|
| 55 | PET Imaging of Pancreatic Dopamine D ₂ and D ₃ Receptor Density with ¹¹ C-(+)-PHNO in Type 1 Diabetes. Journal of Nuclear Medicine, 2020, 61, 570-576. | 5.0 | 19 |
| 56 | Atlas-Based Multiorgan Segmentation for Dynamic Abdominal PET. IEEE Transactions on Radiation and Plasma Medical Sciences, 2020, 4, 50-62. | 3.7 | 14 |
| 57 | Assessment of a white matter reference region for ¹¹ C-UCB-J PET quantification. Journal of Cerebral Blood Flow and Metabolism, 2020, 40, 1890-1901. | 4.3 | 77 |
| 58 | Norepinephrine transporter availability in brown fat is reduced in obesity: a human PET study with [11C] MRB. International Journal of Obesity, 2020, 44, 964-967. | 3.4 | 18 |
| 59 | Measuring the effects of ketamine on mGluR5 using [¹⁸ F]FPEB and PET. Journal of Cerebral Blood Flow and Metabolism, 2020, 40, 2254-2264. | 4.3 | 13 |
| 60 | In vivo 5-HT6 and 5-HT2A receptor availability in antipsychotic treated schizophrenia patients vs. unmedicated healthy humans measured with [11C]GSK215083 PET. Psychiatry Research - Neuroimaging, 2020, 295, 111007. | 1.8 | 17 |
| 61 | Reduced synaptic vesicle protein 2A binding in temporal lobe epilepsy: A [¹¹ C]UCB†positron emission tomography study. Epilepsia, 2020, 61, 2183-2193. | 5.1 | 51 |
| 62 | [¹¹ C]Methionine and [¹¹ C]PBR28 as PET Imaging Tracers to Differentiate Metastatic Tumor Recurrence or Radiation Necrosis. Molecular Imaging, 2020, 19, 153601212096866. | 1.4 | 12 |
| 63 | The rate of dasotraline brain entry is slow following intravenous administration. Psychopharmacology, 2020, 237, 3435-3446. | 3.1 | 1 |
| 64 | In vivo measurement of widespread synaptic loss and associated tau accumulation in early Alzheimer's disease. Alzheimer's and Dementia, 2020, 16, e037791. | 0.8 | 1 |
| 65 | PBR28 Brain PET imaging with lipopolysaccharide challenge for the study of microglia function in Alzheimer's disease. Alzheimer's and Dementia, 2020, 16, e037792. | 0.8 | 0 |
| 66 | The aging rhesus macaque as a potential model for Alzheimer's disease/dementia: An in vivo study of [11 C]PIB, [11 C]UCBâ€j, [18 F]MKâ€6240 and working memory performance. Alzheimer's and Dementia, 2020, 16, e038467. | 0.8 | 0 |
| 67 | ICAâ€derived sources of synaptic density PET ([11 C]UCBâ€J) relate to cognitive impairment severity in Alzheimer's disease. Alzheimer's and Dementia, 2020, 16, e041197. | 0.8 | 3 |
| 68 | 11Câ€PBR28 brain PET imaging with lipopolysaccharide challenge for the study of microglia function in Alzheimer's disease. Alzheimer's and Dementia, 2020, 16, e043584. | 0.8 | 0 |
| 69 | Association between cerebral amyloid accumulation and synaptic density in Alzheimer's disease: A multitracer PET study. Alzheimer's and Dementia, 2020, 16, e043631. | 0.8 | 0 |
| 70 | Association between cerebrospinal fluid biomarkers of neurodegeneration and PET measurements of synaptic density in Alzheimer's disease. Alzheimer's and Dementia, 2020, 16, e044211. | 0.8 | 2 |
| 71 | Validation of a simplified tissueâ€toâ€reference ratio measurement using SUVR for the assessment of synaptic density alterations in Alzheimer's disease using [11 C]UCBâ€J PET. Alzheimer's and Dementia, 2020, 16, e045928. | 0.8 | 1 |
| 72 | In vivo measurement of widespread synaptic loss in Alzheimer's disease with SV2A PET. Alzheimer's and Dementia, 2020, 16, 974-982. | 0.8 | 170 |

| # | Article | IF | CITATIONS |
|----|---|------|-----------|
| 73 | PTSD is associated with neuroimmune suppression: evidence from PET imaging and postmortem transcriptomic studies. Nature Communications, 2020, 11, 2360. | 12.8 | 56 |
| 74 | Kinetic Modeling and Test–Retest Reproducibility of ¹¹ C-EKAP and ¹¹ C-FEKAP, Novel Agonist Radiotracers for PET Imaging of the lº-Opioid Receptor in Humans. Journal of Nuclear Medicine, 2020, 61, 1636-1642. | 5.0 | 10 |
| 75 | Body Mass Index and Age Effects on Brain 11β-Hydroxysteroid Dehydrogenase Type 1: a Positron Emission Tomography Study. Molecular Imaging and Biology, 2020, 22, 1124-1131. | 2.6 | 9 |
| 76 | Guidelines for the content and format of PET brain data in publications and archives: A consensus paper. Journal of Cerebral Blood Flow and Metabolism, 2020, 40, 1576-1585. | 4.3 | 47 |
| 77 | Synthesis and Preclinical Evaluation of an ¹⁸ F-Labeled Synaptic Vesicle Glycoprotein 2A PET Imaging Probe: [¹⁸ F]SynVesT-2. ACS Chemical Neuroscience, 2020, 11, 592-603. | 3.5 | 34 |
| 78 | Synaptic Changes in Parkinson Disease Assessed with in vivo Imaging. Annals of Neurology, 2020, 87, 329-338. | 5.3 | 112 |
| 79 | PET imaging of mGluR5 in Alzheimer's disease. Alzheimer's Research and Therapy, 2020, 12, 15. | 6.2 | 29 |
| 80 | Tobacco Smoking in People Is Not Associated with Altered 18-kDa Translocator Protein Levels: A PET Study. Journal of Nuclear Medicine, 2020, 61, 1200-1204. | 5.0 | 8 |
| 81 | Data-Driven Motion Detection and Event-by-Event Correction for Brain PET: Comparison with Vicra. Journal of Nuclear Medicine, 2020, 61, 1397-1403. | 5.0 | 32 |
| 82 | Inverse changes in raphe and cortical 5â€HT 1B receptor availability after acute tryptophan depletion in healthy human subjects. Synapse, 2020, 74, e22159. | 1.2 | 9 |
| 83 | Separating dopamine D2 and D3 receptor sources of [11C]-(+)-PHNO binding potential: Independent component analysis of competitive binding. NeuroImage, 2020, 214, 116762. | 4.2 | 9 |
| 84 | Human adult and adolescent biodistribution and dosimetry of the synaptic vesicle glycoprotein 2A radioligand 11C-UCB-J. EJNMMI Research, 2020, 10, 83. | 2.5 | 8 |
| 85 | Assessment of population-based input functions for Patlak imaging of whole body dynamic 18F-FDG PET. EJNMMI Physics, 2020, 7, 67. | 2.7 | 45 |
| 86 | Quantitative Cerebral Blood Flow with PET in the 1980s: Going with the Flow (perspective on "Brain) Tj ETQ | 5.0 | 1 |
| 87 | Journal of Nuclear Medicine, 2020, 61, 89S-104S. Reply: 11C-(+)-PHNO Trapping Reversibility for Quantitative PET Imaging of β-Cell Mass in Patients with Type 1 Diabetes. Journal of Nuclear Medicine, 2020, 61, 1693-1693. | 5.0 | 0 |
| 88 | In vivo imaging of D2 receptors and corticosteroids predict behavioural responses to captivity stress in a wild bird. Scientific Reports, 2019, 9, 10407. | 3.3 | 3 |
| 89 | Effects of age, BMI and sex on the glial cell marker TSPO — a multicentre [11C]PBR28 HRRT PET study. European Journal of Nuclear Medicine and Molecular Imaging, 2019, 46, 2329-2338. | 6.4 | 70 |
| 90 | Anti-edema and antioxidant combination therapy for ischemic stroke via glyburide-loaded betulinic acid nanoparticles. Theranostics, 2019, 9, 6991-7002. | 10.0 | 54 |

| # | Article | IF | CITATIONS |
|-----|--|-------|-----------|
| 91 | S13. IN VIVO EVIDENCE OF REDUCED SYNAPTIC VESICLE DENSITY IN SCHIZOPHRENIA USING [11C] UCB-J PET IMAGING. Schizophrenia Bulletin, 2019, 45, S310-S311. | 4.3 | 0 |
| 92 | Data-driven voluntary body motion detection and non-rigid event-by-event correction for static and dynamic PET. Physics in Medicine and Biology, 2019, 64, 065002. | 3.0 | 32 |
| 93 | Human Positron Emission Tomography Neuroimaging. Annual Review of Biomedical Engineering, 2019, 21, 551-581. | 12.3 | 48 |
| 94 | Synthesis and in vivo evaluation of [18F]UCB-J for PET imaging of synaptic vesicle glycoprotein 2A (SV2A). European Journal of Nuclear Medicine and Molecular Imaging, 2019, 46, 1952-1965. | 6.4 | 38 |
| 95 | In Vivo Synaptic Density Imaging with ¹¹ C-UCB-J Detects Treatment Effects of Saracatinib in a Mouse Model of Alzheimer Disease. Journal of Nuclear Medicine, 2019, 60, 1780-1786. | 5.0 | 57 |
| 96 | 142. Synaptic Density Alterations are Associated With Depression Severity and Network Alterations. Biological Psychiatry, 2019, 85, S59. | 1.3 | 4 |
| 97 | Kappa-opioid receptors, dynorphin, and cocaine addiction: a positron emission tomography study. Neuropsychopharmacology, 2019, 44, 1720-1727. | 5.4 | 36 |
| 98 | In vivo evidence for dysregulation of mGluR5 as a biomarker of suicidal ideation. Proceedings of the National Academy of Sciences of the United States of America, 2019, 116, 11490-11495. | 7.1 | 34 |
| 99 | REGION-SPECIFIC ATROPHY AS MEASURED BY CORTICAL GRAY MATTER VOLUME IS ASSOCIATED WITH BOTH REGIONAL AND TOTAL CORTICAL AMYLOID-BETA BURDEN IN COGNITIVELY NORMAL INDIVIDUALS AT RISK FOR ALZHEIMER'S DISEASE. American Journal of Geriatric Psychiatry, 2019, 27, S186-S187. | 1.2 | 1 |
| 100 | Brain-Dedicated Emission Tomography Systems: A Perspective on Requirements for Clinical Research and Clinical Needs in Brain Imaging. IEEE Transactions on Radiation and Plasma Medical Sciences, 2019, 3, 254-261. | 3.7 | 17 |
| 101 | Imaging the Enzyme 11β-Hydroxysteroid Dehydrogenase Type 1 with PET: Evaluation of the Novel Radiotracer ¹¹ C-AS2471907 in Human Brain. Journal of Nuclear Medicine, 2019, 60, 1140-1146. | 5.0 | 11 |
| 102 | Event-by-event non-rigid data-driven PET respiratory motion correction methods: comparison of principal component analysis and centroid of distribution. Physics in Medicine and Biology, 2019, 64, 165014. | 3.0 | 11 |
| 103 | Social status and demographic effects of the kappa opioid receptor: a PET imaging study with a novel agonist radiotracer in healthy volunteers. Neuropsychopharmacology, 2019, 44, 1714-1719. | 5.4 | 22 |
| 104 | A singleâ€center, openâ€label positron emission tomography study to evaluate brivaracetam and levetiracetam synaptic vesicle glycoprotein 2A binding in healthy volunteers. Epilepsia, 2019, 60, 958-967. | 5.1 | 45 |
| 105 | Lower synaptic density is associated with depression severity and network alterations. Nature Communications, 2019, 10, 1529. | 12.8 | 277 |
| 106 | Evaluation of ¹¹ C-LSN3172176 as a Novel PET Tracer for Imaging M ₁ Muscarinic Acetylcholine Receptors in Nonhuman Primates. Journal of Nuclear Medicine, 2019, 60, 1147-1153. | 5.0 | 17 |
| 107 | P4â€481: ASSOCIATION BETWEEN ENTORHINAL CORTICAL TAU ACCUMULATION AND HIPPOCAMPAL SYNAPTIC DENSITY IN OLDER INDIVIDUALS WITH NORMAL COGNITION AND EARLY ALZHEIMER'S DISEASE: PRELIMINARY EXPERIENCE. Alzheimer's and Dementia, 2019, 15, P1497. | 0.8 | 0 |
| 108 | ICâ€₽â€140: ASSOCIATION BETWEEN MGLUR5 AND SYNAPTIC DENSITY: A MULTIâ€TRACER STUDY IN HEALTHY / AND ALZHEIMER'S DISEASE. Alzheimer's and Dementia, 2019, 15, P115. | AGING | 0 |

| # | Article | IF | CITATIONS |
|-----|---|-----|-----------|
| 109 | F33. In Vivo Brain Imaging of 11beta-Hydroxysteroid Dehydrogenase, a Marker of Cortisol Production, in PTSD. Biological Psychiatry, 2019, 85, S225. | 1.3 | Ο |
| 110 | Synthesis and <i>in Vivo</i> Evaluation of a Novel PET Radiotracer for Imaging of Synaptic Vesicle Glycoprotein 2A (SV2A) in Nonhuman Primates. ACS Chemical Neuroscience, 2019, 10, 1544-1554. | 3.5 | 70 |
| 111 | Quantitative PET Imaging in Drug Development: Estimation of Target Occupancy. Bulletin of Mathematical Biology, 2019, 81, 3508-3541. | 1.9 | 21 |
| 112 | Respiratory Motion Compensation for PET/CT with Motion Information Derived from Matched Attenuation-Corrected Gated PET Data. Journal of Nuclear Medicine, 2018, 59, 1480-1486. | 5.0 | 54 |
| 113 | Evaluation of Pancreatic VMAT2 Binding with Active and Inactive Enantiomers of [18F]FP-DTBZ in Healthy Subjects and Patients with Type 1 Diabetes. Molecular Imaging and Biology, 2018, 20, 835-845. | 2.6 | 24 |
| 114 | Simplified Quantification and Acquisition Protocol for ¹²³ I-MIBG Dynamic SPECT. Journal of Nuclear Medicine, 2018, 59, 1574-1580. | 5.0 | 5 |
| 115 | F188. Preliminary Evidence for mGluR5 Dysregulation in Borderline Personality Disorder and Relationship to Suicidal Behavior. Biological Psychiatry, 2018, 83, S312. | 1.3 | 2 |
| 116 | Age-Related Change in 5-HT ₆ Receptor Availability in Healthy Male Volunteers Measured with ¹¹ C-GSK215083 PET. Journal of Nuclear Medicine, 2018, 59, 1445-1450. | 5.0 | 34 |
| 117 | Evaluation of PET Brain Radioligands for Imaging Pancreatic β-Cell Mass: Potential Utility of 11C-(+)-PHNO. Journal of Nuclear Medicine, 2018, 59, 1249-1254. | 5.0 | 22 |
| 118 | Investigation of Sub-Centimeter Lung Nodule Quantification for Low-Dose PET. IEEE Transactions on Radiation and Plasma Medical Sciences, 2018, 2, 41-50. | 3.7 | 6 |
| 119 | Dose-Related Target Occupancy and Effects on Circuitry, Behavior, and Neuroplasticity of the Glycine Transporter-1 Inhibitor PF-03463275 in Healthy and Schizophrenia Subjects. Biological Psychiatry, 2018, 84, 413-421. | 1.3 | 43 |
| 120 | Non-Rigid Event-by-Event Continuous Respiratory Motion Compensated List-Mode Reconstruction for PET. IEEE Transactions on Medical Imaging, 2018, 37, 504-515. | 8.9 | 33 |
| 121 | Decreased VMAT2 in the pancreas of humans with type 2 diabetes mellitus measured in vivo by PET imaging. Diabetologia, 2018, 61, 2598-2607. | 6.3 | 18 |
| 122 | A 3D-printed modular device for imaging the brain of small birds. Journal of Neuroscience Methods, 2018, 293, 183-190. | 2.5 | 6 |
| 123 | Evaluation of the Lysophosphatidic Acid Receptor Type 1 Radioligand ¹¹ C-BMT-136088 for Lung Imaging in Rhesus Monkeys. Journal of Nuclear Medicine, 2018, 59, 327-333. | 5.0 | 16 |
| 124 | Cortical β-amyloid burden, gray matter, and memory in adults at varying APOE ε4 risk for Alzheimer's disease. Neurobiology of Aging, 2018, 61, 207-214. | 3.1 | 28 |
| 125 | Cardiacâ€gated parametric images from ⁸² Rb <scp>PET</scp> from dynamic frames and direct 4D reconstruction. Medical Physics, 2018, 45, 639-654. | 3.0 | 9 |
| 126 | Evaluation of (â€)â€{ ¹⁸ <scp>F]F</scp> lubatineâ€specific binding: Implications for reference region approaches. Synapse, 2018, 72, e22016. | 1.2 | 7 |

| # | Article | IF | CITATIONS |
|-----|--|-----|-----------|
| 127 | Kinetic evaluation and test–retest reproducibility of [¹¹ C]UCB-J, a novel radioligand for positron emission tomography imaging of synaptic vesicle glycoprotein 2A in humans. Journal of Cerebral Blood Flow and Metabolism, 2018, 38, 2041-2052. | 4.3 | 143 |
| 128 | P2â€365: PET IMAGING OF SYNAPTIC DENSITY (SYNAPTIC VESICLE GLYCOPROTEIN 2A, SV2A) IN ALZHEIMER'S DISEASE: INITIAL EXPERIENCE. Alzheimer's and Dementia, 2018, 14, P832. | 0.8 | 0 |
| 129 | P1â€469: PET IMAGING OF METABOTROPIC GLUTAMATE RECEPTOR 5 BINDING IN ALZHEIMER'S DISEASE. Alzheimer's and Dementia, 2018, 14, P501. | 0.8 | 1 |
| 130 | ICâ€04â€03: PET IMAGING OF METABOTROPIC GLUTAMATE RECEPTOR 5 BINDING IN ALZHEIMER'S DISEASE. Alzheimer's and Dementia, 2018, 14, P8. | 0.8 | 0 |
| 131 | ICâ€Pâ€183: PET IMAGING OF SYNAPTIC DENSITY (SYNAPTIC VESICLE GLYCOPROTEIN 2A, SV2A) IN ALZHEIMER'S DISEASE: INITIAL EXPERIENCE. Alzheimer's and Dementia, 2018, 14, P152. | 0.8 | 0 |
| 132 | Initial Experience with PET Imaging of Synaptic Density (SV2A) in Alzheimer's Disease: A New Biomarker for Clinical Trials?. American Journal of Geriatric Psychiatry, 2018, 26, S145-S146. | 1.2 | 3 |
| 133 | F149. Preliminary Evidence for Altered Synaptic Density and a Possible Role for Accelerated Ageing in Individuals With MDD as Measured With [11C]UCB-J PET. Biological Psychiatry, 2018, 83, S296. | 1.3 | 4 |
| 134 | F3. Imaging Alpha7 Nicotinic Acetylcholine Receptors in Individuals With PTSD. Biological Psychiatry, 2018, 83, S237-S238. | 1.3 | 0 |
| 135 | Kappa opioid receptor binding in major depression: A pilot study. Synapse, 2018, 72, e22042. | 1.2 | 26 |
| 136 | InÂVivo Reactive Oxygen Species Detection With a Novel Positron Emission Tomography Tracer, 18F-DHMT, Allows for Early Detection of Anthracycline-Induced Cardiotoxicity in Rodents. JACC Basic To Translational Science, 2018, 3, 378-390. | 4.1 | 46 |
| 137 | Assessing Synaptic Density in Alzheimer Disease With Synaptic Vesicle Glycoprotein 2A Positron Emission Tomographic Imaging. JAMA Neurology, 2018, 75, 1215. | 9.0 | 304 |
| 138 | Improved discrimination between benign and malignant LDCT screening-detected lung nodules with dynamic over static ¹⁸ F-FDG PET as a function of injected dose. Physics in Medicine and Biology, 2018, 63, 175015. | 3.0 | 17 |
| 139 | Clinical and scientific value in the pursuit of quantification of beta cells in the pancreas by PET imaging. Diabetologia, 2018, 61, 2671-2673. | 6.3 | 6 |
| 140 | High Single Doses of Radiation May Induce Elevated Levels of Hypoxia in Early-Stage Non-Small Cell Lung Cancer Tumors. International Journal of Radiation Oncology Biology Physics, 2018, 102, 174-183. | 0.8 | 36 |
| 141 | Noradrenergic Activity in the Human Brain: A Mechanism Supporting the Defense Against Hypoglycemia. Journal of Clinical Endocrinology and Metabolism, 2018, 103, 2244-2252. | 3.6 | 23 |
| 142 | Novel Use of Agent 11C-PHNO for Pet CT Imaging of Pancreatic Beta-Cell Mass. Diabetes, 2018, 67, . | 0.6 | 0 |
| 143 | Determination of receptor occupancy in the presence of mass dose: [11C]GSK189254 PET imaging of histamine H3 receptor occupancy by PF-03654746. Journal of Cerebral Blood Flow and Metabolism, 2017, 37, 1095-1107. | 4.3 | 31 |
| 144 | Regional and source-based patterns of [11 C]-(+)-PHNO binding potential reveal concurrent alterations in dopamine D 2 and D 3 receptor availability in cocaine-use disorder. NeuroImage, 2017, 148, 343-351. | 4.2 | 32 |

0

| # | Article | IF | CITATIONS |
|-----|---|-----|-----------|
| 145 | Experimentally reducing corticosterone mitigates rapid captivity effects on behavior, but not body composition, in a wild bird. Hormones and Behavior, 2017, 89, 121-129. | 2.1 | 29 |
| 146 | PET imaging of α7 nicotinic acetylcholine receptors: a comparative study of [18F]ASEM and [18F]DBT-10 in nonhuman primates, and further evaluation of [18F]ASEM in humans. European Journal of Nuclear Medicine and Molecular Imaging, 2017, 44, 1042-1050. | 6.4 | 47 |
| 147 | Metabotropic Glutamate Receptor 5 and Glutamate Involvement in Major Depressive Disorder: A Multimodal Imaging Study. Biological Psychiatry: Cognitive Neuroscience and Neuroimaging, 2017, 2, 449-456. | 1.5 | 47 |
| 148 | Quantification of Tumor Hypoxic Fractions Using Positron Emission Tomography with [18F]Fluoromisonidazole ([18F]FMISO) Kinetic Analysis and Invasive Oxygen Measurements. Molecular Imaging and Biology, 2017, 19, 893-902. | 2.6 | 17 |
| 149 | PET Imaging for Early Detection of Alzheimer's Disease. PET Clinics, 2017, 12, 329-350. | 3.0 | 44 |
| 150 | Data-driven event-by-event respiratory motion correction using TOF PET list-mode centroid of distribution. Physics in Medicine and Biology, 2017, 62, 4741-4755. | 3.0 | 44 |
| 151 | The Search for a Subtype-Selective PET Imaging Agent for the GABA _A Receptor Complex: Evaluation of the Radiotracer [¹¹ C]ADO in Nonhuman Primates. Molecular Imaging, 2017, 16, 153601211773125. | 1.4 | 8 |
| 152 | Altered metabotropic glutamate receptor 5 markers in PTSD: In vivo and postmortem evidence. Proceedings of the National Academy of Sciences of the United States of America, 2017, 114, 8390-8395. | 7.1 | 107 |
| 153 | 18. In Vivo Quantification of mGluR5 Availability in Posttraumatic Stress Disorder. Biological Psychiatry, 2017, 81, S8. | 1.3 | 0 |
| 154 | 389. In Vivo Evidence of Lower Synaptic Density in Depression and Associated Mood and Cognitive Deficits: A [11C]UCB-J PET Imaging Study. Biological Psychiatry, 2017, 81, S159. | 1.3 | 3 |
| 155 | 962. In-vivo Evidence of Decreased Synaptic Density in Schizophrenia: A [11C]UCB-J PET Imaging Study. Biological Psychiatry, 2017, 81, S389. | 1.3 | 7 |
| 156 | Trends in Radiation Medical Sciences: Instrumentation and Imaging Algorithms. IEEE Transactions on Radiation and Plasma Medical Sciences, 2017, 1, 201-205. | 3.7 | 2 |
| 157 | Direct reconstruction of parametric images for brain PET with event-by-event motion correction: evaluation in two tracers across count levels. Physics in Medicine and Biology, 2017, 62, 5344-5364. | 3.0 | 17 |
| 158 | InÂvivo variation in same-day estimates of metabotropic glutamate receptor subtype 5 binding using [¹¹ C]ABP688 and [¹⁸ F]FPEB. Journal of Cerebral Blood Flow and Metabolism, 2017, 37, 2716-2727. | 4.3 | 49 |
| 159 | Quantitative projection of human brain penetration of the H ₃ antagonist PF-03654746 by integrating rat-derived brain partitioning and PET receptor occupancy. Xenobiotica, 2017, 47, 119-126. | 1.1 | 5 |
| 160 | Microglial depletion and activation: A [11C]PBR28 PET study in nonhuman primates. EJNMMI Research, 2017, 7, 59. | 2.5 | 39 |
| 161 | Accounting for Breathing Pattern Variability in Event-by-Event Respiratory Motion Correction in PET Using Dynamic Internal-External Motion Correlation. , 2017, , . | | 1 |

162 Strategies to Improve Direct EM Patlak Reconstructions. , 2017, , .

| # | Article | IF | CITATIONS |
|-----|--|------|-----------|
| 163 | GPU-based List-mode Direct Parametric Reconstruction for Dynamic Cardiac SPECT. , 2017, , . | | 1 |
| 164 | Estradiol modulates neural response to conspecific and heterospecific song in female house sparrows: An in vivo positron emission tomography study. PLoS ONE, 2017, 12, e0182875. | 2.5 | 16 |
| 165 | Direct EM reconstruction of parametric images from list-mode brain PET using a novel model based on logan graphical analysis. , 2016, , . | | 3 |
| 166 | Nicotine and Nicotine Abstinence Do Not Interfere with GABA _A Receptor Neuroadaptations During Alcohol Abstinence. Alcoholism: Clinical and Experimental Research, 2016, 40, 698-705. | 2.4 | 5 |
| 167 | Comparative evaluation of two glycine transporter 1 radiotracers [11C]GSK931145 and [18F]MK-6577 in baboons. Synapse, 2016, 70, 112-120. | 1.2 | 4 |
| 168 | Quantification of myocardial blood flow with 82Rb: Validation with 15O-water using time-of-flight and point-spread-function modeling. EJNMMI Research, 2016, 6, 68. | 2.5 | 34 |
| 169 | Preclinical Evaluation of ¹⁸ F-PF-05270430, a Novel PET Radioligand for the Phosphodiesterase 2A Enzyme. Journal of Nuclear Medicine, 2016, 57, 1448-1453. | 5.0 | 13 |
| 170 | Event-by-Event Continuous Respiratory Motion Correction for Dynamic PET Imaging. Journal of Nuclear Medicine, 2016, 57, 1084-1090. | 5.0 | 39 |
| 171 | Quantitative Analysis of Dynamic ¹²³ I-mIBG SPECT Imaging Data in Healthy Humans with a Population-Based Metabolite Correction Method. Journal of Nuclear Medicine, 2016, 57, 1226-1232. | 5.0 | 17 |
| 172 | First-in-Human Assessment of the Novel PDE2A PET Radiotracer ¹⁸ F-PF-05270430. Journal of Nuclear Medicine, 2016, 57, 1388-1395. | 5.0 | 27 |
| 173 | Evaluation of pancreatic VMAT2 binding with active and inactive enantiomers of 18 F-FP-DTBZ in baboons. Nuclear Medicine and Biology, 2016, 43, 743-751. | 0.6 | 20 |
| 174 | Elevated Dopamine D2/3 Receptor Availability in Obese Individuals: A PET Imaging Study with [11C](+)PHNO. Neuropsychopharmacology, 2016, 41, 3042-3050. | 5.4 | 47 |
| 175 | Brivaracetam, a selective highâ€affinity synaptic vesicle protein 2A (<scp>SV</scp> 2A) ligand with preclinical evidence of high brain permeability and fast onset of action. Epilepsia, 2016, 57, 201-209. | 5.1 | 130 |
| 176 | Preferential binding to dopamine D3 over D2 receptors by cariprazine in patients with schizophrenia using PET with the D3/D2 receptor ligand [11C]-(+)-PHNO. Psychopharmacology, 2016, 233, 3503-3512. | 3.1 | 101 |
| 177 | Imaging synaptic density in the living human brain. Science Translational Medicine, 2016, 8, 348ra96. | 12.4 | 343 |
| 178 | Age-related changes in binding of the D2/3 receptor radioligand [11C](+)PHNO in healthy volunteers. NeuroImage, 2016, 130, 241-247. | 4.2 | 43 |
| 179 | Receptor Occupancy of the Â-Opioid Antagonist LY2456302 Measured with Positron Emission Tomography and the Novel Radiotracer 11C-LY2795050. Journal of Pharmacology and Experimental Therapeutics, 2016, 356, 260-266. | 2.5 | 47 |
| 180 | Reduced Brain Cannabinoid Receptor Availability in Schizophrenia. Biological Psychiatry, 2016, 79, 997-1005. | 1.3 | 83 |

| # | Article | IF | CITATIONS |
|-----|---|------|-----------|
| 181 | OCD is associated with an altered association between sensorimotor gating and cortical and subcortical 5-HT1b receptor binding. Journal of Affective Disorders, 2016, 196, 87-96. | 4.1 | 38 |
| 182 | Rapid Changes in Cannabinoid 1 Receptor Availability in Cannabis-Dependent Male Subjects After Abstinence From Cannabis. Biological Psychiatry: Cognitive Neuroscience and Neuroimaging, 2016, 1, 60-67. | 1.5 | 135 |
| 183 | Synthesis and Preclinical Evaluation of ¹¹ C-UCB-J as a PET Tracer for Imaging the Synaptic Vesicle Clycoprotein 2A in the Brain. Journal of Nuclear Medicine, 2016, 57, 777-784. | 5.0 | 197 |
| 184 | Increased Nanoparticle Delivery to Brain Tumors by Autocatalytic Priming for Improved Treatment and Imaging. ACS Nano, 2016, 10, 4209-4218. | 14.6 | 103 |
| 185 | PET imaging evaluation of [18F]DBT-10, a novel radioligand specific to α7 nicotinic acetylcholine receptors, in nonhuman primates. European Journal of Nuclear Medicine and Molecular Imaging, 2016, 43, 537-547. | 6.4 | 20 |
| 186 | Abdominal multi-organ segmentation of dynamic PET studies using modified fuzzy clustering algorithm. , 2015, , . | | 2 |
| 187 | P3-143: Amyloid burden is associated with decreased gray matter volume but not episodic memory performance in cognitively normal first-degree relatives at varying ApoE4 risk for Alzheimer's disease. , 2015, 11, P680-P681. | | 0 |
| 188 | Further evaluation of [11C]MP-10 as a radiotracer for phosphodiesterase 10A: PET imaging study in rhesus monkeys and brain tissue metabolite analysis. Synapse, 2015, 69, 86-95. | 1.2 | 18 |
| 189 | Assessment of kinetic modeling quality of fit by cluster analysis of residuals: Application to direct reconstruction of cardiac PET data. , 2015, , . | | 3 |
| 190 | Test–Retest Reproducibility of Binding Parameters in Humans with ¹¹ C-LY2795050, an Antagonist PET Radiotracer for the κ Opioid Receptor. Journal of Nuclear Medicine, 2015, 56, 243-248. | 5.0 | 35 |
| 191 | IC-P-101: Amyloid burden is associated with decreased gray matter volume but not episodic memory performance in cognitively normal first-degree relatives at varying ApoE4 risk for Alzheimer's disease. , 2015, 11, P69-P69. | | 0 |
| 192 | In Vivo Ketamine-Induced Changes in [11 C]ABP688 Binding to Metabotropic Glutamate Receptor Subtype 5. Biological Psychiatry, 2015, 77, 266-275. | 1.3 | 82 |
| 193 | Deficits in Prefrontal Cortical and Extrastriatal Dopamine Release in Schizophrenia. JAMA Psychiatry, 2015, 72, 316. | 11.0 | 304 |
| 194 | Evaluation of [18 F]-(-)-norchlorofluorohomoepibatidine ([18 F]-(-)-NCFHEB) as a PET radioligand to image the nicotinic acetylcholine receptors in non-human primates. Nuclear Medicine and Biology, 2015, 42, 570-577. | 0.6 | 17 |
| 195 | Imaging human brown adipose tissue under room temperature conditions with 11C-MRB, a selective norepinephrine transporter PET ligand. Metabolism: Clinical and Experimental, 2015, 64, 747-755. | 3.4 | 25 |
| 196 | Test–retest reliability of the novel 5-HT1B receptor PET radioligand [11C]P943. European Journal of Nuclear Medicine and Molecular Imaging, 2015, 42, 468-477. | 6.4 | 20 |
| 197 | 11C-PBR28 imaging in multiple sclerosis patients and healthy controls: test-retest reproducibility and focal visualization of active white matter areas. European Journal of Nuclear Medicine and Molecular Imaging, 2015, 42, 1081-1092. | 6.4 | 77 |
| 198 | Imaging robust microglial activation after lipopolysaccharide administration in humans with PET. Proceedings of the National Academy of Sciences of the United States of America, 2015, 112, 12468-12473. | 7.1 | 265 |

| # | Article | IF | CITATIONS |
|-----|--|------|-----------|
| 199 | Measurement of <i>B</i> _{max} and <i>K</i> _d with the Glycine Transporter 1 Radiotracer ¹⁸ F-MK6577 using a Novel Multi-Infusion Paradigm. Journal of Cerebral Blood Flow and Metabolism, 2015, 35, 2001-2009. | 4.3 | 10 |
| 200 | Imaging the Cannabinoid CB1 Receptor in Humans with [¹¹ C] OMAR: Assessment of Kinetic Analysis Methods, Test–Retest Reproducibility, and Gender Differences. Journal of Cerebral Blood Flow and Metabolism, 2015, 35, 1313-1322. | 4.3 | 79 |
| 201 | Test–retest reproducibility of the metabotropic glutamate receptor 5 ligand [18F]FPEB with bolus plus constant infusion in humans. European Journal of Nuclear Medicine and Molecular Imaging, 2015, 42, 1530-1541. | 6.4 | 37 |
| 202 | A preliminary study of dopamine D2/3 receptor availability and social status in healthy and cocaine dependent humans imaged with [11C](+)PHNO. Drug and Alcohol Dependence, 2015, 154, 167-173. | 3.2 | 25 |
| 203 | Tobacco smoking interferes with GABA _A receptor neuroadaptations during prolonged alcohol withdrawal. Proceedings of the National Academy of Sciences of the United States of America, 2014, 111, 18031-18036. | 7.1 | 21 |
| 204 | Association of In Vivo κ-Opioid Receptor Availability and the Transdiagnostic Dimensional Expression of Trauma-Related Psychopathology. JAMA Psychiatry, 2014, 71, 1262. | 11.0 | 67 |
| 205 | Imaging Nicotine- and Amphetamine-Induced Dopamine Release in Rhesus Monkeys with [11C]PHNO vs [11C]raclopride PET. Neuropsychopharmacology, 2014, 39, 866-874. | 5.4 | 43 |
| 206 | Radiolabeling of Poly(lactic- <i>co</i> -glycolic acid) (PLGA) Nanoparticles with Biotinylated F-18 Prosthetic Groups and Imaging of Their Delivery to the Brain with Positron Emission Tomography. Bioconjugate Chemistry, 2014, 25, 2157-2165. | 3.6 | 45 |
| 207 | Evaluation of the sensitivity of the novel α4β2* nicotinic acetylcholine receptor PET radioligand ¹⁸ Fâ€(â€)â€NCFHEB to increases in synaptic acetylcholine levels in rhesus monkeys. Synapse, 2014, 68, 556-564. | 1.2 | 21 |
| 208 | Kinetic Modeling of 11C-LY2795050, A Novel Antagonist Radiotracer for PET Imaging of the Kappa Opioid Receptor in Humans. Journal of Cerebral Blood Flow and Metabolism, 2014, 34, 1818-1825. | 4.3 | 42 |
| 209 | An Improved Antagonist Radiotracer for the Î ^e -Opioid Receptor: Synthesis and Characterization of 11C-LY2459989. Journal of Nuclear Medicine, 2014, 55, 1185-1191. | 5.0 | 26 |
| 210 | Evaluation of ¹¹ C-BU99008, a PET Ligand for the Imidazoline ₂ Binding Sites in Rhesus Brain. Journal of Nuclear Medicine, 2014, 55, 838-844. | 5.0 | 44 |
| 211 | Phosphodiesterase 10A PET Radioligand Development Program: From Pig to Human. Journal of Nuclear Medicine, 2014, 55, 595-601. | 5.0 | 50 |
| 212 | Biodistribution and Radiation Dosimetry of LMI1195: First-in-Human Study of a Novel ¹⁸ F-Labeled Tracer for Imaging Myocardial Innervation. Journal of Nuclear Medicine, 2014, 55, 1445-1451. | 5.0 | 91 |
| 213 | Evaluation of Frame-Based and Event-by-Event Motion-Correction Methods for Awake Monkey Brain PET Imaging. Journal of Nuclear Medicine, 2014, 55, 287-293. | 5.0 | 12 |
| 214 | Imaging Glutamate Homeostasis in Cocaine Addiction with the Metabotropic Glutamate Receptor 5 Positron Emission Tomography Radiotracer [11C]ABP688 and Magnetic Resonance Spectroscopy. Biological Psychiatry, 2014, 75, 165-171. | 1.3 | 66 |
| 215 | Dopamine D3 receptor alterations in cocaine-dependent humans imaged with [11C](+)PHNO. Drug and Alcohol Dependence, 2014, 139, 100-105. | 3.2 | 63 |
| 216 | Reductions in Brain 5-HT1B Receptor Availability in Primarily Cocaine-Dependent Humans. Biological Psychiatry, 2014, 76, 816-822. | 1.3 | 50 |

| # | Article | IF | CITATIONS |
|-----|--|------|-----------|
| 217 | Decreased norepinephrine transporter availability in obesity: Positron Emission Tomography imaging with (S,S)-[11C]O-methylreboxetine. NeuroImage, 2014, 86, 306-310. | 4.2 | 41 |
| 218 | Parametric Imaging and Test–Retest Variability of ¹¹ C-(+)-PHNO Binding to D ₂ /D ₃ Dopamine Receptors in Humans on the High-Resolution Research Tomograph PET Scanner. Journal of Nuclear Medicine, 2014, 55, 960-966. | 5.0 | 38 |
| 219 | Evaluation of the agonist PET radioligand [11C]GR103545 to image kappa opioid receptor in humans: Kinetic model selection, test–retest reproducibility and receptor occupancy by the antagonist PF-04455242. Neurolmage, 2014, 99, 69-79. | 4.2 | 54 |
| 220 | Direct EM reconstruction of kinetic parameters from list-mode cardiac PET. , 2014, , . | | 9 |
| 221 | Data-driven respiratory motion estimation and correction using TOF PET list-mode centroid of distribution. , 2014, , . | | 3 |
| 222 | The neuroinflammation marker translocator protein is not elevated in individuals with mild-to-moderate depression: A [11C]PBR28 PET study. Brain, Behavior, and Immunity, 2013, 33, 131-138. | 4.1 | 180 |
| 223 | Direct, Quantitative, and Noninvasive Imaging of the Transport of Active Agents Through Intact Brain with Positron Emission Tomography. Molecular Imaging and Biology, 2013, 15, 596-605. | 2.6 | 4 |
| 224 | Reduced post-synaptic serotonin type 1A receptor binding in bipolar depression. European Neuropsychopharmacology, 2013, 23, 822-829. | 0.7 | 30 |
| 225 | Association of Posttraumatic Stress Disorder With Reduced In Vivo Norepinephrine Transporter Availability in the Locus Coeruleus. JAMA Psychiatry, 2013, 70, 1199. | 11.0 | 116 |
| 226 | Studies of the metabotropic glutamate receptor 5 radioligand [¹¹ C]ABP688 with <i>N</i> -acetylcysteine challenge in rhesus monkeys. Synapse, 2013, 67, 489-501. | 1.2 | 42 |
| 227 | Feasible uniform-resolution penalized likelihood reconstruction for static- and multi-frame 3D PET. , 2013, , . | | 0 |
| 228 | Effect of subsets on bias and variance in low-count iterative PET reconstruction. , 2013, , . | | 1 |
| 229 | List-Mode PET Motion Correction Using Markerless Head Tracking: Proof-of-Concept With Scans of Human Subject. IEEE Transactions on Medical Imaging, 2013, 32, 200-209. | 8.9 | 55 |
| 230 | In Hot Blood. JACC: Cardiovascular Imaging, 2013, 6, 569-573. | 5.3 | 17 |
| 231 | Synthesis and Evaluation of 11C-LY2795050 as a \hat{I}^2 -Opioid Receptor Antagonist Radiotracer for PET Imaging. Journal of Nuclear Medicine, 2013, 54, 455-463. | 5.0 | 80 |
| 232 | Kinetic Analysis of Drug–Target Interactions with PET for Characterization of Pharmacological Hysteresis. Journal of Cerebral Blood Flow and Metabolism, 2013, 33, 700-707. | 4.3 | 13 |
| 233 | Optimization of PET–MR registrations for nonhuman primates using mutual information measures: A Multi-Transform Method (MTM). NeuroImage, 2013, 64, 571-581. | 4.2 | 26 |
| 234 | List-mode reconstruction for the Biograph mCT with physics modeling and event-by-event motion correction. Physics in Medicine and Biology, 2013, 58, 5567-5591. | 3.0 | 47 |

| # | Article | lF | CITATIONS |
|-----|--|-----|-----------|
| 235 | Eventâ€byâ€event respiratory motion correction for PET with 3D internalâ€1D external motion correlation. Medical Physics, 2013, 40, 112507. | 3.0 | 27 |
| 236 | Determination of the In Vivo Selectivity of a New κ-Opioid Receptor Antagonist PET Tracer ¹¹ C-LY2795050 in the Rhesus Monkey. Journal of Nuclear Medicine, 2013, 54, 1668-1674. | 5.0 | 34 |
| 237 | Tracer Kinetic Modeling of [¹¹ C]AFM, a New PET Imaging Agent for the Serotonin Transporter. Journal of Cerebral Blood Flow and Metabolism, 2013, 33, 1886-1896. | 4.3 | 17 |
| 238 | Awake Nonhuman Primate Brain PET Imaging with Minimal Head Restraint: Evaluation of GABA _A -Benzodiazepine Binding with ¹¹ C-Flumazenil in Awake and Anesthetized Animals. Journal of Nuclear Medicine, 2013, 54, 1962-1968. | 5.0 | 19 |
| 239 | Imaging Changes in Synaptic Acetylcholine Availability in Living Human Subjects. Journal of Nuclear Medicine, 2013, 54, 78-82. | 5.0 | 33 |
| 240 | Determination of In Vivo <i>B</i> _{max} and <i>K</i> _d for ¹¹ C-GR103545, an Agonist PET Tracer for κ-Opioid Receptors: A Study in Nonhuman Primates. Journal of Nuclear Medicine, 2013, 54, 600-608. | 5.0 | 31 |
| 241 | Cerebral blood flow with [¹⁵ 0]water PET studies using an image-derived input function and MR-defined carotid centerlines. Physics in Medicine and Biology, 2013, 58, 1903-1923. | 3.0 | 51 |
| 242 | Kinetic Analysis of the Metabotropic Glutamate Subtype 5 Tracer [¹⁸ F]FPEB in Bolus and Bolus-Plus-Constant-Infusion Studies in Humans. Journal of Cerebral Blood Flow and Metabolism, 2013, 33, 532-541. | 4.3 | 61 |
| 243 | Highly penetrative, drug-loaded nanocarriers improve treatment of glioblastoma. Proceedings of the National Academy of Sciences of the United States of America, 2013, 110, 11751-11756. | 7.1 | 222 |
| 244 | Evaluation of motion correction methods in human brain PET imaging—A simulation study based on human motion data. Medical Physics, 2013, 40, 102503. | 3.0 | 83 |
| 245 | Test-retest reproducibility of [11C]-(+)-propyl-hexahydro-naphtho-oxazin positron emission tomography using the bolus plus constant infusion paradigm. Molecular Imaging, 2013, 12, 77-82. | 1.4 | 13 |
| 246 | Event-by-event respiratory motion correction for PET with 3-Dimensional internal-external motion correlation. , 2012, , . | | 5 |
| 247 | Myocardial blood flow from dynamic PET using Independent Component Analysis. , 2012, , . | | 1 |
| 248 | Uniform Spatial resolution list mode reconstruction for the HRRT. , 2012, , . | | 1 |
| 249 | Yale Center for Clinical Investigation: Leveraging Industry Partnerships and Research Cores. Clinical and Translational Science, 2012, 5, 435-436. | 3.1 | Ο |
| 250 | List-mode reconstruction for the FOCUS-220 with motion correction and spatially-variant probability density functions: Application to awake monkey imaging. , 2012, , . | | 0 |
| 251 | Dynamic assessment of head motion compensation for the HRRT. , 2012, , . | | 0 |
| 252 | List-mode reconstruction for the Biograph mCT with probabilistic line-of-response positioning and event-by-event motion correction. , 2012, , . | | 3 |

| # | Article | IF | CITATIONS |
|-----|---|-----|-----------|
| 253 | Assessment of a three-dimensional line-of-response probability density function system matrix for PET. Physics in Medicine and Biology, 2012, 57, 6827-6848. | 3.0 | 18 |
| 254 | Age Effects on Serotonin Receptor 1B as Assessed by PET. Journal of Nuclear Medicine, 2012, 53, 1411-1414. | 5.0 | 26 |
| 255 | Glucose Metabolism in the Insula and Cingulate Is Affected by Systemic Inflammation in Humans. Journal of Nuclear Medicine, 2012, 53, 601-607. | 5.0 | 100 |
| 256 | In Vivo Imaging of Endogenous Pancreatic β-Cell Mass in Healthy and Type 1 Diabetic Subjects Using ¹⁸ F-Fluoropropyl-Dihydrotetrabenazine and PET. Journal of Nuclear Medicine, 2012, 53, 908-916. | 5.0 | 108 |
| 257 | Direct 4-D PET List Mode Parametric Reconstruction With a Novel EM Algorithm. IEEE Transactions on Medical Imaging, 2012, 31, 2213-2223. | 8.9 | 42 |
| 258 | Widespread abnormality of the Î ³ -aminobutyric acid-ergic system in Tourette syndrome. Brain, 2012, 135, 1926-1936. | 7.6 | 166 |
| 259 | Positron Emission Tomography Shows Elevated Cannabinoid <scp>CB</scp> ₁ Receptor Binding in Men with Alcohol Dependence. Alcoholism: Clinical and Experimental Research, 2012, 36, 2104-2109. | 2.4 | 53 |
| 260 | Endotoxin-induced systemic inflammation activates microglia: [11C]PBR28 positron emission tomography in nonhuman primates. NeuroImage, 2012, 63, 232-239. | 4.2 | 179 |
| 261 | Ex Vivo and In Vivo Evaluation of the Norepinephrine Transporter Ligand [11C]MRB for Brown Adipose Tissue Imaging. Nuclear Medicine and Biology, 2012, 39, 1081-1086. | 0.6 | 31 |
| 262 | Affinity and selectivity of [¹¹ C]â€(+)â€₱HNO for the D3 and D2 receptors in the rhesus monkey brain in vivo. Synapse, 2012, 66, 489-500. | 1.2 | 74 |
| 263 | Reduced Amygdala Serotonin Transporter Binding in Posttraumatic Stress Disorder. Biological Psychiatry, 2011, 70, 1033-1038. | 1.3 | 79 |
| 264 | Evaluation of [11C]MRB for assessment of occupancy of norepinephrine transporters: Studies with atomoxetine in non-human primates. NeuroImage, 2011, 56, 268-279. | 4.2 | 50 |
| 265 | Radiosynthesis and in vivo evaluation of [11C]MP-10 as a positron emission tomography radioligand for phosphodiesterase 10A. Nuclear Medicine and Biology, 2011, 38, 875-884. | 0.6 | 42 |
| 266 | Lateralization and gender differences in the dopaminergic response to unpredictable reward in the human ventral striatum. European Journal of Neuroscience, 2011, 33, 1706-1715. | 2.6 | 82 |
| 267 | Pancreatic Beta Cell Mass PET Imaging and Quantification with [11C]DTBZ and [18F]FP-(+)-DTBZ in Rodent Models of Diabetes. Molecular Imaging and Biology, 2011, 13, 973-984. | 2.6 | 54 |
| 268 | Assessing the sensitivity of [¹¹ C]p943, a novel 5â€HT _{IB} radioligand, to endogenous serotonin release. Synapse, 2011, 65, 1113-1117. | 1.2 | 21 |
| 269 | Recovery from chronic spinal cord contusion after nogo receptor intervention. Annals of Neurology, 2011, 70, 805-821. | 5.3 | 87 |
| | | | |

270 Validation of the spatially variant probability density functions for the HRRT. , 2011, , .

3

| # | Article | IF | CITATIONS |
|-----|--|------|-----------|
| 271 | The Effect of Early Trauma Exposure on Serotonin Type 1B Receptor Expression Revealed by Reduced Selective Radioligand Binding. Archives of General Psychiatry, 2011, 68, 892. | 12.3 | 84 |
| 272 | Arterial transit time effects in pulsed arterial spin labeling CBF mapping: Insight from a PET and MR study in normal human subjects. Magnetic Resonance in Medicine, 2010, 63, 374-384. | 3.0 | 58 |
| 273 | PET imaging of the effects of age and cocaine on the norepinephrine transporter in the human brain using (S,S)-[¹¹ C]O-methylreboxetine and HRRT. Synapse, 2010, 64, 30-38. | 1.2 | 112 |
| 274 | Kinetic Modeling of the Serotonin 5-HT _{1B} Receptor Radioligand [¹¹ C]P943 in Humans. Journal of Cerebral Blood Flow and Metabolism, 2010, 30, 196-210. | 4.3 | 83 |
| 275 | Quantification of Smoking-Induced Occupancy of β2-Nicotinic Acetylcholine Receptors: Estimation of Nondisplaceable Binding. Journal of Nuclear Medicine, 2010, 51, 1226-1233. | 5.0 | 33 |
| 276 | Multiple acquisition frame-based motion correction for awake monkey PET imaging. , 2010, , . | | 2 |
| 277 | Evaluation of direct 4D parametric reconstruction with low count human PET data. , 2010, , . | | 1 |
| 278 | Segmentation of rat spinal cord in PET using spatiotemporal information. , 2010, , . | | 0 |
| 279 | Count-rate dependent resolution degradation from pulse pile-up on the HRRT. , 2010, , . | | 6 |
| 280 | Evaluation of a 3D point spread function (PSF) model derived from Monte Carlo simulation for a small animal PET scanner. Proceedings of SPIE, 2010, , . | 0.8 | 0 |
| 281 | Serotonin 1B Receptor Imaging in Alcohol Dependence. Biological Psychiatry, 2010, 67, 800-803. | 1.3 | 69 |
| 282 | Effects of Early-Life Stress on Serotonin1A Receptors in Juvenile Rhesus Monkeys Measured by Positron Emission Tomography. Biological Psychiatry, 2010, 67, 1146-1153. | 1.3 | 71 |
| 283 | Clinically Relevant Doses of Methylphenidate Significantly Occupy Norepinephrine Transporters in Humans In Vivo. Biological Psychiatry, 2010, 68, 854-860. | 1.3 | 201 |
| 284 | PET evaluation of the TSPO ligands [F-18]FEPPA, [F-18]PRB06, and [F-18]PBR111 in nonhuman primate. NeuroImage, 2010, 52, S147. | 4.2 | 0 |
| 285 | Kinetic modeling of the mGluR5 tracer [18F]F-FPEB in humans. NeuroImage, 2010, 52, S169-S170. | 4.2 | 1 |
| 286 | Kinetic analysis of the kappa agonist tracer [11C]GR103545 in healthy controls. NeuroImage, 2010, 52, S172. | 4.2 | 2 |
| 287 | Awake nonhuman primate brain PET imaging without head restraint. NeuroImage, 2010, 52, S18. | 4.2 | 1 |
| 288 | High-resolution imaging of brain 5-HT1B receptors in the rhesus monkey using [11C]P943. Nuclear Medicine and Biology, 2010, 37, 205-214. | 0.6 | 40 |

| # | Article | IF | CITATIONS |
|-----|---|------|-----------|
| 289 | Accuracy of head motion compensation for the HRRT: Comparison of methods. , 2009, 2009, 3199-3202. | | 6 |
| 290 | Initial evaluation of direct 4D parametric reconstruction with human PET data. , 2009, 2009, 2503-2506. | | 7 |
| 291 | A multimodal approach to image-derived input functions for brain PET. , 2009, 2009, 2710-2714. | | 12 |
| 292 | Imaging incorporation of circulating docosahexaenoic acid into the human brain using positron emission tomography. Journal of Lipid Research, 2009, 50, 1259-1268. | 4.2 | 156 |
| 293 | Dopamine D3 receptor antagonists: The quest for a potentially selective PET ligand. Part 3: Radiosynthesis and in vivo studies. Bioorganic and Medicinal Chemistry Letters, 2009, 19, 5056-5059. | 2.2 | 24 |
| 294 | Noninvasive Estimation of Normalized Distribution Volume: Application to the Muscarinic-2 Ligand [18F]FP-TZTP. Journal of Cerebral Blood Flow and Metabolism, 2008, 28, 420-430. | 4.3 | 19 |
| 295 | Imaging Neuroinflammation in Alzheimer's Disease with Radiolabeled Arachidonic Acid and PET. Journal of Nuclear Medicine, 2008, 49, 1414-1421. | 5.0 | 158 |
| 296 | Direct 4D list mode parametric reconstruction for PET with a novel EM algorithm. , 2008, 4774103, 3625-3628. | | 19 |
| 297 | Altered Cerebral γ-Aminobutyric Acid Type A–Benzodiazepine Receptor Binding in Panic Disorder Determined by [11C]Flumazenil Positron Emission Tomography. Archives of General Psychiatry, 2008, 65, 1166. | 12.3 | 103 |
| 298 | Quantitative accuracy of HRRT lIST-MODE reconstructions: Effect of low statistics. , 2008, 2008, 5121-5124. | | 13 |
| 299 | Task-Related Interaction between Basal Ganglia and Cortical Dopamine Release. Journal of Neuroscience, 2007, 27, 14434-14441. | 3.6 | 41 |
| 300 | Imaging signal transduction via arachidonic acid in the human brain during visual stimulation, by means of positron emission tomography. NeuroImage, 2007, 34, 1342-1351. | 4.2 | 39 |
| 301 | Count-Rate Dependent Component-Based Normalization for the HRRT. IEEE Transactions on Nuclear Science, 2007, 54, 486-495. | 2.0 | 22 |
| 302 | Consensus Nomenclature for in vivo Imaging of Reversibly Binding Radioligands. Journal of Cerebral Blood Flow and Metabolism, 2007, 27, 1533-1539. | 4.3 | 1,840 |
| 303 | Consensus nomenclature: its time has come. European Journal of Nuclear Medicine and Molecular Imaging, 2007, 34, 1239-1239. | 6.4 | 10 |
| 304 | Cerebral blood flow in temporal lobe epilepsy: a partial volume correction study. European Journal of Nuclear Medicine and Molecular Imaging, 2007, 34, 2066-2072. | 6.4 | 6 |
| 305 | Long-Term Clinical Improvement in MPTP-Lesioned Primates after Gene Therapy with AAV-hAADC. Molecular Therapy, 2006, 14, 564-570. | 8.2 | 249 |
| 306 | Cerebral Metabolic Effects of Intravenous Glycine in Healthy Human Subjects. Journal of Clinical Psychopharmacology, 2006, 26, 595-599. | 1.4 | 12 |

| # | Article | IF | CITATIONS |
|-----|---|------|-----------|
| 307 | Reduced Muscarinic Type 2 Receptor Binding in Subjects With Bipolar Disorder. Archives of General Psychiatry, 2006, 63, 741. | 12.3 | 106 |
| 308 | Age and APOE-ε4 genotype influence the effect of physostigmine infusion on the in-vivo distribution volume of the muscarinic-2-receptor dependent tracer [18F]FP-TZTP. Synapse, 2006, 60, 86-92. | 1.2 | 18 |
| 309 | The Effect of Antiepileptic Drugs on 5-HT1A-Receptor Binding Measured by Positron Emission Tomography. Epilepsia, 2006, 47, 499-503. | 5.1 | 57 |
| 310 | Measurement of Regional Rates of Cerebral Protein Synthesis with L-[1-11C]leucine and PET with Correction for Recycling of Tissue Amino Acids: II. Validation in Rhesus Monkeys. Journal of Cerebral Blood Flow and Metabolism, 2005, 25, 629-640. | 4.3 | 42 |
| 311 | No Change in Serotonin Type 1A Receptor Binding in Patients With Posttraumatic Stress Disorder. American Journal of Psychiatry, 2005, 162, 383-385. | 7.2 | 70 |
| 312 | Tracer Kinetic Modeling in PET. , 2005, , 127-159. | | 91 |
| 313 | Differential effects of paroxetine on raphe and cortical 5-HT1A binding: A PET study in monkeys. NeuroImage, 2005, 28, 238-248. | 4.2 | 27 |
| 314 | 5-HT 1A receptors are reduced in temporal lobe epilepsy after partial-volume correction. Journal of Nuclear Medicine, 2005, 46, 1128-35. | 5.0 | 92 |
| 315 | Nicotine-Induced Dopamine Release in Primates Measured with [11C]Raclopride PET. Neuropsychopharmacology, 2004, 29, 259-268. | 5.4 | 57 |
| 316 | Reduced Serotonin Type 1A Receptor Binding in Panic Disorder. Journal of Neuroscience, 2004, 24, 589-591. | 3.6 | 350 |
| 317 | Toward an evolutionary perspective on conceptual representation: Species-specific calls activate visual and affective processing systems in the macaque. Proceedings of the National Academy of Sciences of the United States of America, 2004, 101, 17516-17521. | 7.1 | 118 |
| 318 | Caloric restriction increases neurotrophic factor levels and attenuates neurochemical and behavioral deficits in a primate model of Parkinson's disease. Proceedings of the National Academy of Sciences of the United States of America, 2004, 101, 18171-18176. | 7.1 | 334 |
| 319 | A Potential Cholinergic Mechanism of Procaine's Limbic Activation. Neuropsychopharmacology, 2004, 29, 1239-1250. | 5.4 | 23 |
| 320 | Species-specific calls evoke asymmetric activity in the monkey's temporal poles. Nature, 2004, 427, 448-451. | 27.8 | 324 |
| 321 | Brain incorporation of 11C-arachidonic acid, blood volume, and blood flow in healthy aging: a study with partial-volume correction. Journal of Nuclear Medicine, 2004, 45, 1471-9. | 5.0 | 76 |
| 322 | In vivo muscarinic 2 receptor imaging in cognitively normal young and older volunteers. Synapse, 2003, 48, 39-44. | 1.2 | 64 |
| 323 | Higher in vivo muscarinic-2 receptor distribution volumes in aging subjects with an apolipoprotein E-?4 allele. Synapse, 2003, 49, 150-156. | 1.2 | 59 |
| 324 | Brain Uptake of the Acid Metabolites of F-18—Labeled WAY 100635 Analogs. Journal of Cerebral Blood Flow and Metabolism, 2003, 23, 249-260. | 4.3 | 44 |

| # | Article | IF | CITATIONS |
|-----|--|------|-----------|
| 325 | Linearized Reference Tissue Parametric Imaging Methods: Application to [11C]DASB Positron Emission Tomography Studies of the Serotonin Transporter in Human Brain. Journal of Cerebral Blood Flow and Metabolism, 2003, 23, 1096-1112. | 4.3 | 574 |
| 326 | Determination of [18F]FCWAY, [18F]FP-TZTP, and their metabolites in plasma using rapid and efficient liquid-liquid and solid phase extractions. Nuclear Medicine and Biology, 2003, 30, 233-240. | 0.6 | 23 |
| 327 | Brain Uptake of the Acid Metabolites of F-18???Labeled WAY 100635 Analogs. Journal of Cerebral Blood Flow and Metabolism, 2003, , 249-260. | 4.3 | 19 |
| 328 | Brain Incorporation of [¹¹ C]Arachidonic Acid in Young Healthy Humans Measured with Positron Emission Tomography. Journal of Cerebral Blood Flow and Metabolism, 2002, 22, 1453-1462. | 4.3 | 63 |
| 329 | Noise Reduction in the Simplified Reference Tissue Model for Neuroreceptor Functional Imaging. Journal of Cerebral Blood Flow and Metabolism, 2002, 22, 1440-1452. | 4.3 | 353 |
| 330 | Strategies to Improve Neuroreceptor Parameter Estimation by Linear Regression Analysis. Journal of Cerebral Blood Flow and Metabolism, 2002, 22, 1271-1281. | 4.3 | 286 |
| 331 | Reduced prefrontal activity predicts exaggerated striatal dopaminergic function in schizophrenia. Nature Neuroscience, 2002, 5, 267-271. | 14.8 | 603 |
| 332 | Scatchard Analysis with Bolus/Infusion Administration of [11C]Raclopride. , 2002, , 63-69. | | 3 |
| 333 | Strategies to Improve Neuroreceptor Parameter Estimation by Linear Regression Analysis. Journal of Cerebral Blood Flow and Metabolism, 2002, , 1271-1281. | 4.3 | 84 |
| 334 | Noise Reduction in the Simplified Reference Tissue Model for Neuroreceptor Functional Imaging. Journal of Cerebral Blood Flow and Metabolism, 2002, , 1440-1452. | 4.3 | 110 |
| 335 | Brain Incorporation of [11C]Arachidonic Acid in Young Healthy Humans Measured With Positron Emission Tomography. Journal of Cerebral Blood Flow and Metabolism, 2002, , 1453-1462. | 4.3 | 27 |
| 336 | Device-dependent activity estimation and decay correction of radionuclide mixtures with application to Tc-94m PET studies. Medical Physics, 2001, 28, 36-45. | 3.0 | 12 |
| 337 | Amphetamine-Induced Dopamine Release. , 2001, , 205-209. | | 12 |
| 338 | [α-11C]Methyl-l-tryptophan in Anesthetized Rhesus Monkeys. , 2001, , 229-235. | | 1 |
| 339 | Opiate receptor avidity in the thalamus is sexually dimorphic in the elderly. Synapse, 2000, 38, 226-229. | 1.2 | 13 |
| 340 | Synthesis and evaluation of an 18F analog of forskolin for imaging adenylyl cyclase. Journal of Fluorine Chemistry, 2000, 101, 297-304. | 1.7 | 13 |
| 341 | The Suitability of [11C]-α-Methyl-L-tryptophan as a Tracer for Serotonin Synthesis: Studies With Dual Administration of [11C] and [14C] Labeled Tracer. Journal of Cerebral Blood Flow and Metabolism, 2000, 20, 244-252. | 4.3 | 74 |
| 342 | Kinetic Analysis of the 5-HT2A Ligand [11C]MDL 100,907. Journal of Cerebral Blood Flow and Metabolism, 2000, 20, 899-909. | 4.3 | 78 |

| # | Article | IF | CITATIONS |
|-----|---|------|-----------|
| 343 | Opiate receptor avidity is increased in rhesus monkeys following unilateral optic tract lesion combined with transections of corpus callosum and hippocampal and anterior commissures. Brain Research, 2000, 879, 1-6. | 2.2 | 4 |
| 344 | PET evaluation of [18F]FCWAY, an analog of the 5-HT1A receptor antagonist, WAY-100635. Nuclear Medicine and Biology, 2000, 27, 493-497. | 0.6 | 71 |
| 345 | Pet physiological measurements using constant infusion. Nuclear Medicine and Biology, 2000, 27, 657-660. | 0.6 | 83 |
| 346 | Comparison of PET [150]Water Studies with 6-Minute and 10-Minute InterScan Intervals: Single-Subject and Group Analyses. Journal of Cerebral Blood Flow and Metabolism, 1999, 19, 570-582. | 4.3 | 17 |
| 347 | Bolus Injection versus Slow Infusion of [150]Water for Positron Emission Tomography Activation Studies. Journal of Cerebral Blood Flow and Metabolism, 1999, 19, 843-852. | 4.3 | 9 |
| 348 | In vivo muscarinic binding of 3-(alkylthio)-3-thiadiazolyl tetrahydropyridines. Synapse, 1999, 31, 29-40. | 1.2 | 30 |
| 349 | Opiate receptor avidity is reduced bilaterally in rhesus monkeys unilaterally lesioned with MPTP. , 1999, 33, 282-288. | | 10 |
| 350 | Using single photon emission tomography (SPECT) and positron emission tomography (PET) to trace the distribution of muscarinic acetylcholine receptor (MACHR) binding radioligands. Life Sciences, 1999, 64, 511-518. | 4.3 | 12 |
| 351 | Development of Fluorine-18-Labeled 5-HT1AAntagonists. Journal of Medicinal Chemistry, 1999, 42, 1576-1586. | 6.4 | 112 |
| 352 | Positron Emission Tomography [150]Water Studies with Short InterScan Interval for Single-Subject and Group Analysis: Influence of Background Subtraction. Journal of Cerebral Blood Flow and Metabolism, 1998, 18, 433-444. | 4.3 | 18 |
| 353 | Muscarinic Cholinergic Receptor Measurements with [18F]FP-TZTP: Control and Competition Studies. Journal of Cerebral Blood Flow and Metabolism, 1998, 18, 1130-1142. | 4.3 | 98 |
| 354 | Assessment of Dynamic Neurotransmitter Changes with Bolus or Infusion Delivery of Neuroreceptor Ligands. Journal of Cerebral Blood Flow and Metabolism, 1998, 18, 1196-1210. | 4.3 | 72 |
| 355 | Opiate receptor avidity is reduced in non-motor impaired MPTP-lesioned rhesus monkeys. Brain Research, 1998, 806, 292-296. | 2.2 | 15 |
| 356 | Brain Serotonin Synthesis Rates in Rhesus Monkeys Determined by [11C]α-Methyl-?-Tryptophan and Positron Emission Tomography Compared to CSF 5-Hydroxyindole-3-Acetic Acid Concentrations. Neuropsychopharmacology, 1998, 19, 345-353. | 5.4 | 37 |
| 357 | Dissociated Pattern of Activity in Visual Cortices and Their Projections During Human Rapid Eye Movement Sleep. Science, 1998, 279, 91-95. | 12.6 | 584 |
| 358 | Axial slice width in 3D PET: characterization and potential improvement with axial interleaving. Physics in Medicine and Biology, 1998, 43, 921-928. | 3.0 | 5 |
| 359 | Characteristics of Neurotransmitter Competition Studies Using Constant Infusion of Tracer 1 1Transcripts of the BRAINPET97 discussion of this chapter can be found in Section VIII , 1998, , 435-439. | | 0 |
| 360 | Opiate receptor avidity and cerebral blood flow in Alzheimer's disease. Journal of the Neurological Sciences, 1997, 148, 171-180. | 0.6 | 47 |

| # | Article | IF | CITATIONS |
|-----|--|-----|-----------|
| 361 | In vivo muscarinic binding selectivity of QNB. Bioorganic and Medicinal Chemistry, 1997, 5, 1555-1567. | 3.0 | 17 |
| 362 | Quantification of Amphetamine-Induced Changes in [11C]Raclopride Binding with Continuous Infusion. Journal of Cerebral Blood Flow and Metabolism, 1997, 17, 437-447. | 4.3 | 237 |
| 363 | Optimization of Noninvasive Activation Studies with 15O-Water and Three-Dimensional Positron Emission Tomography. Journal of Cerebral Blood Flow and Metabolism, 1997, 17, 732-739. | 4.3 | 22 |
| 364 | Kinetic Modeling of [11C]Raclopride: Combined PET-Microdialysis Studies. Journal of Cerebral Blood Flow and Metabolism, 1997, 17, 932-942. | 4.3 | 183 |
| 365 | Quantification and pharmacokinetics of blood-brain barrier disruption in humans. Journal of Neurosurgery, 1996, 85, 1056-1065. | 1.6 | 98 |
| 366 | Hyperosmolar blood-brain barrier disruption in baboons: an in vivo study using positron emission tomography and rubidium-82. Journal of Neurosurgery, 1996, 84, 494-502. | 1.6 | 26 |
| 367 | Absolute Cerebral Blood Flow with [150]Water and PET. , 1996, , 185-190. | | 7 |
| 368 | The Functional Neuroanatomy of Tourette's Syndrome: An FDG-PET Study. II: Relationships between Regional Cerebral Metabolism and Associated Behavioral and Cognitive Features of the Illness. Neuropsychopharmacology, 1995, 13, 151-168. | 5.4 | 75 |
| 369 | A kinetic comparison of [18F]2-fluoro-2-deoxyglucose and [18F]2-fluoro-2-deoxymannose using positron emission tomography. Nuclear Medicine and Biology, 1994, 21, 857-863. | 0.6 | 5 |
| 370 | Analysis of Covariance in Statistical Parametric Mapping. Journal of Cerebral Blood Flow and Metabolism, 1993, 13, 1038-1038. | 4.3 | 11 |
| 371 | Comparison of Bolus and Infusion Methods for Receptor Quantitation: Application to [¹⁸ F]Cyclofoxy and Positron Emission Tomography. Journal of Cerebral Blood Flow and Metabolism, 1993, 13, 24-42. | 4.3 | 343 |
| 372 | Reproducibility of Resting Cerebral Blood Flow Measurements with H ₂ ¹⁵ O Positron Emission Tomography in Humans. Journal of Cerebral Blood Flow and Metabolism, 1993, 13, 748-754. | 4.3 | 75 |
| 373 | Activation of cerebral blood flow during a visuoperceptual task in patients with Alzheimer-type dementia. Neurobiology of Aging, 1993, 14, 35-44. | 3.1 | 103 |
| 374 | The Functional Neuroanatomy of Tourette's Syndrome: An FDG-PET Study. I. Regional Changes in Cerebral Glucose Metabolism Differentiating Patients and Controls. Neuropsychopharmacology, 1993, 9, 277-291. | 5.4 | 166 |
| 375 | Dissociation of Object and Spatial Vision in Human Extrastriate Cortex: Age-Related Changes in Activation of Regional Cerebral Blood Flow Measured with [15 O]Water and Positron Emission Tomography. Journal of Cognitive Neuroscience, 1992, 4, 23-34. | 2.3 | 140 |
| 376 | PET imaging of opiate receptor binding in human epilepsy using [18F]cyclofoxy. Epilepsy Research, 1992, 13, 129-139. | 1.6 | 68 |
| 377 | Distribution and Kinetics of 3-O-Methyl-6-[18F]fluoro-L-DOPA in the Rhesus Monkey Brain. Journal of Cerebral Blood Flow and Metabolism, 1991, 11, 726-734. | 4.3 | 49 |
| 378 | Precision and Accuracy Considerations of Physiological Quantitation in PET. Journal of Cerebral Blood Flow and Metabolism, 1991, 11, A45-A50. | 4.3 | 34 |

| # | Article | IF | CITATIONS |
|-----|--|-----|-----------|
| 379 | Intravascular streaming during carotid artery infusions. Journal of Neurosurgery, 1991, 74, 763-772. | 1.6 | 59 |
| 380 | Brain Glucose Metabolism in Noninsulin-Dependent Diabetes Mellitus: A Study in Pima Indians Using Positron Emission Tomography during Hyperinsulinemia with Euglycemic Glucose Clamp. Journal of Clinical Endocrinology and Metabolism, 1990, 71, 1602-1610. | 3.6 | 32 |
| 381 | A Realistic Computer-Simulated Brain Phantom for Evaluation of PET Charactenstics. IEEE Transactions on Medical Imaging, 1987, 6, 250-257. | 8.9 | 12 |
| 382 | Examination of Blood — Brain Barrier Permeability in Dementia of the Alzheimer Type with [⁶⁸ Ga]EDTA and Positron Emission Tomography. Journal of Cerebral Blood Flow and Metabolism, 1987, 7, 1-8. | 4.3 | 129 |
| 383 | III. Biomathematical Aspects of Physiological Brain Imaging. Journal of Cerebral Blood Flow and Metabolism, 1987, 7, S11-S13. | 4.3 | 3 |
| 384 | A Maximum Likelihood Method for Region-of-Interest Evaluation in Emission Tomography. Journal of Computer Assisted Tomography, 1986, 10, 654-663. | 0.9 | 96 |
| 385 | Weighted Integration Method for Local Cerebral Blood Flow Measurements with Positron Emission Tomography. Journal of Cerebral Blood Flow and Metabolism, 1986, 6, 245-258. | 4.3 | 106 |
| 386 | A Noninvasive Positron Computed Tomography Technique Using Oxygen-15-Labeled Water for the Evaluation of Neurobehavioral Task Batteries. Journal of Cerebral Blood Flow and Metabolism, 1985, 5, 70-78. | 4.3 | 171 |
| 387 | An Efficient Algorithm for Reconsiruction of SPECT Images in the Presence of Spatially Varying Attenuation. IEEE Transactions on Nuclear Science, 1985, 32, 1190-1197. | 2.0 | 1 |
| 388 | Theoretical Analysis of Optimal Conditions in Fquilibrium Imaging of in Vivo Receptors. IEEE Transactions on Nuclear Science, 1985, 32, 1496-1502. | 2.0 | 2 |
| 389 | Comment: The EM Parametric Image Reconstruction Algorithm. Journal of the American Statistical Association, 1985, 80, 20-22. | 3.1 | 79 |
| 390 | A Statistical Model for Positron Emission Tomography: Comment. Journal of the American Statistical Association, 1985, 80, 20. | 3.1 | 42 |
| 391 | Multiple-Radionuclide Autoradiography in Evaluation of Cerebral Function. Journal of Cerebral Blood Flow and Metabolism, 1984, 4, 264-269. | 4.3 | 31 |
| 392 | Cerebral Glucose Metabolism as a Function of Age in Man: Influence of the Rate Constants in the Fluorodeoxyglucose Method. Journal of Cerebral Blood Flow and Metabolism, 1983, 3, 250-253. | 4.3 | 75 |
| 393 | Tracer Kinetic Modeling in Positron Computed Tomography. Lecture Notes in Biomathematics, 1983, , 298-344. | 0.3 | 2 |
| 394 | All Analysis of Signal Amplification Using Small Detectors in Positron Emission Tomography. Journal of Computer Assisted Tomography, 1982, 6, 551-565. | 0.9 | 80 |
| 395 | Tomographic mapping of human cerebral metabolism: Sensory deprivation. Annals of Neurology, 1982, 12, 435-444. | 5.3 | 127 |
| 396 | Measurement of Local Blood Flow and Distribution Volume with Short-Lived Isotopes: A General Input Technique. Journal of Cerebral Blood Flow and Metabolism, 1982, 2, 99-108. | 4.3 | 123 |